J. Fluid Mech. (1988), *vol.* 188, *pp.* 383–410
Printed in Great Britain

Numerical shock propagation in non-uniform media

By D. W. SCHWENDEMAN
Department of Mathematical Sciences, Rensselaer Polytechnic Institute, Troy NY 12180-3590, USA

(Received 24 October 1986)

A general numerical scheme is developed to calculate the motion of shock waves in gases with non-uniform properties. The numerical scheme is based on the approximatc theory of geometrical shock dynamics. The refracted shockfronts at both planar and curved gas interfaces are calculated. Both regular and irregular refraction patterns are obtained, and in particular, precursor-irregular refraction systems are found using the approximate theory. The numerical results are compared with recent theoretical and experimental investigations. It is shown that the shockfronts determined using geometrical shock dynamics are in good agreement with the actual shock waves.

1. Introduction

In our recent paper, Henshaw, Smyth & Schwendeman (1986), a numerical scheme was introduced and used to calculate the motion of shock waves in gases, based on the approximate theory of geometrical shock dynamics (Whitham 1957, 1959). This earlier work dealt with problems for which the shock wave propagated into a gas with uniform properties. In this paper, we shall be concerned with the more general problem of shock-wave motion in gases with non-uniform properties. Of main interest will be the bending and distortion of the leading shockfront as it propagates into a non-uniform gas. The motion of the leading shockfront will be determined using an extended version of the original theory of geometrical shock dynamics. In this approximate theory, the shockfront propagates along rays with its Mach number M adjusted in accordance with the changes in the area A of the ray tubes. The A–M relation for the extended theory is a differential relation that now contains additional terms involving the gradients of the gas non-uniformities. We present the necessary elements of the extended theory in §2.

An efficient method for numerically propagating the shockfront based on the extended theory of geometrical shock dynamics is discussed in §3. We represent the shockfront by a discrete set of points. Each point is advanced along its unit normal with a speed determined by an approximate integration of the differential A–M relation along rays. A mesh refinement scheme is employed to maintain a relatively even point spacing. This refinement scheme is required since the point spacing tends to increase in expansive regions of the shockfront or decrease in compressive regions. A smoothing scheme is used periodically to dampen high-frequency numerical fluctuations in the shockfront position.

The present numerical scheme is designed to propagate the leading shockfront in two dimensions. Axisymmetric problems are calculated using the present numerical

scheme with only minor adjustments required. Shock propagation in three dimensions is being considered for future research.

An important simplification in geometrical shock dynamics is that the shockfront can be calculated directly without explicit knowledge of the flow field behind the shock. Numerically, this implies that only $O(N)$ operations (e.g. multiplications) are required at each time step to propagate a shockfront in *two dimensions*, where $1/N$ is average point spacing along the shockfront. A numerical scheme that determines the shocks from a calculation of the entire two-dimensional flow field would require at least $O(N^2)$ operations per time step to gain the same shockfront resolution. These two-dimensional flow calculations are possible but time-consuming given the current state of computing machines. For shock propagation in *three dimensions*, geometrical shock dynamics would require $O(N^2)$ operations per time step. These calculations are also time-consuming but possible, whereas the corresponding calculations for the entire three-dimensional flow field do not appear to be feasible given the present available computers.

The numerical scheme discussed in §3 is quite general and may be used to propagate shock waves in gases with any prescribed equilibrium distribution of sound speed, pressure, density and specific-heat ratio. In order to demonstrate the use of the numerical scheme, however, we shall only consider examples where the shock wave travels into a gas with a variable sound-speed distribution. Two such problems will be considered in §4: shock-wave refraction at a planar interface separating two gases with different sound speeds and shock-wave refraction at a curved interface.

The results discussed in §4 are compared with data obtained by other theoretical and experimental investigations. Analytic solutions to the equations of geometrical shock dynamics were obtained by Catherasoo & Sturtevant (1983) for the case of shock-wave refraction at a planar interface separating two gases with unequal constant sound speeds. For this special geometry, the shockfronts are self-similar and are composed of centred expansions in Mach number M and ray angle θ along with jumps in M and θ at shock–shocks and at the interface. The shockfronts, in this case, may be constructed analytically using characteristics and jump conditions at shock–shocks and at the interface. This was the method used by Catherasoo & Sturtevant. We use these analytic solutions as a check of the accuracy of our more flexible numerical scheme presented in §3. Other results for this problem were obtained experimentally by Jahn (1956), Abd-el-Fattah, Henderson & Lozzi (1976) and Abd-el-Fattah & Henderson (1978). Catherasoo & Sturtevant showed that these experimental results compared favourably with their solutions determined by geometrical shock dynamics. In particular, they showed that their shockfronts accurately predicted the transition between regular and irregular refraction systems for the actual shocks.

For certain ranges of the problem parameters, Catherasoo & Sturtevant were unable to obtain solutions using their construction method. In one case, the difficulty was due to the formation of a shock–shock on the interface, and in another case, the shockfront became normal to the interface so that no rays crossed it. In the latter case, the limit signalled the onset of a precursor-irregular refraction pattern similar to that which is found in geometrical acoustics. The difficulty in their construction of solutions is that a provisional choice of the form of the solution is required before an iteration procedure can be applied to confirm this choice and obtain the solution. An advantage of our numerical scheme is that no prior knowledge of the solution is required. Furthermore, the correct form of the solution can be obtained from our

numerical calculations and then verified using Catherasoo & Sturtevant's procedure. Using our numerical scheme, we were able to find solutions in both cases that were previously unknown.

The most interesting resolved case showed the existence of precursor-irregular refraction systems for the shockfronts determined using the approximate theory. These precursor-irregular refraction systems occur at a 'slow–fast' interface, depending on the incident shock strength and interface inclination angle, when the transmitted shock travelling in the faster medium 'runs ahead' of the incident shock, thus generating a precursor wave that attaches the two shocks (see figure 7 (*c*, *d*) in §4, for example). The same shock systems were also observed experimentally by Abd-el-Fattah & Henderson (1978). We compare the shock–shock positions found using the approximate theory with the experimental triple-point positions, and it is shown that the two results are in good agreement.

The second problem we consider in §4 is shock-wave refraction at cylindrical and spherical interfaces separating two different gases. These results were motivated by recent experiments performed by Haas & Sturtevant (1987) for the same problem. Depending on the gas properties, the shock converged or diverged in the cylindrical or spherical region. For the divergent case, regular refraction at the curved interface was observed initially with transition to irregular refraction and a pair of triple points (shock–shocks) forming in the surrounding medium at later stages of the interaction. The convergent case, on the other hand, produced a pronounced shock focusing within the cylindrical or spherical regions. These shock-wave refraction systems are seen in our numerical study as well.

2. General theory

Geometrical shock dynamics is an approximate method for propagating the leading shockfront directly without explicitly calculating the flow field behind. The theory assumes that points on the shockfront move along rays normal to the shock with a speed determined by the changes in the shockfront geometry and by the changes in the medium. The numerical scheme (to be discussed in §3) implements this directly and advances the shockfront according to these changes.

2.1. *The A–M relation*

We require some theory for the dependence of the shock Mach number M on the ray tube area A and the parameters of the medium (such as the ambient sound speed). One such theory is an application of Whitham's *characteristic rule* to the one-dimensional formulation for flow in a channel (ray tube) with slowly varying cross-sectional area A (Whitham 1974). We assume that a shock is travelling down the channel with Mach number M into a equilibrium distribution of sound speed a_0, density ρ_0, pressure p_0 and specific heat ratio γ. If σ measures the distance down the channel, the characteristic rule is

$$\frac{\mathrm{d}p}{\mathrm{d}\sigma}+\rho a\frac{\mathrm{d}u}{\mathrm{d}\sigma}+\frac{\rho a^2 u}{u+a}\frac{1}{A}\frac{\mathrm{d}A}{\mathrm{d}\sigma}=\frac{\rho a}{u+a}F, \tag{2.1}$$

where p, ρ, u and a are the pressure, density, velocity and sound speed of the gas just behind the shock, respectively. The quantity F in (2.1) is an acceleration due to some body force (such as gravity) and at equilibrium we have

$$\frac{1}{\rho_0}\frac{\mathrm{d}p_0}{\mathrm{d}\sigma}=F. \tag{2.2}$$

At the moving shock, we can eliminate p, ρ, u and a in favour of M using the normal shock conditions:

$$p = p_0 \frac{2\gamma M^2-(\gamma-1)}{\gamma+1}, \quad \rho = \rho_0 \frac{(\gamma+1)M^2}{(\gamma-1)M^2+2},$$

$$u = a_0 \frac{2(M^2-1)}{(\gamma+1)M}, \quad a^2 = a_0^2 \frac{(2\gamma M^2-(\gamma-1))((\gamma-1)M^2+2)}{(\gamma+1)^2 M^2}.$$

This procedure results in a differential relation between M, A and the various gas parameters at the moving shock of the form

$$\frac{M\lambda(M,\sigma)}{M^2-1}\frac{\mathrm{d}M}{\mathrm{d}\sigma}+\frac{1}{A}\frac{\mathrm{d}A}{\mathrm{d}\sigma} = S(M,\sigma), \tag{2.3}$$

where

$$\lambda(M,\sigma) = \left(1+\frac{2}{\gamma+1}\frac{1-\mu^2}{\mu}\right)\left(1+2\mu+\frac{1}{M^2}\right),$$

$$\mu^2 = \frac{(\gamma-1)M^2+2}{2\gamma M^2-(\gamma-1)},$$

and $S(M,\sigma)$ is a source term which contains the gradients of the gas non-uniformities. Specifically, we have

$$S(M,\sigma) = -g(M,\sigma)\frac{1}{a_0}\frac{\mathrm{d}a_0}{\mathrm{d}\sigma}-h(M,\sigma)\frac{1}{p_0}\frac{\mathrm{d}p_0}{\mathrm{d}\sigma}-k(M,\sigma)\frac{\mathrm{d}\gamma}{\mathrm{d}\sigma}, \tag{2.4}$$

where

$$g(M,\sigma) = 1+\frac{2\mu(M^2-1)}{(\gamma-1)M^2+2},$$

$$h(M,\sigma) = \frac{1}{2\gamma(M^2-1)}\left\{2(M^2-1)+\mu(2\gamma M^2-(\gamma-1))-\frac{(\gamma+1)^2\mu M^2}{(\gamma-1)M^2+2}\right\},$$

$$k(M,\sigma) = \frac{g(M,\sigma)}{\gamma(\gamma+1)}(\mu-\gamma).$$

Henceforth, we shall refer to (2.3) as the A–M relation.

The differential form of the A–M relation given by (2.3) for a non-uniform medium is the same relation as that used by Catherasoo & Sturtevant (1983), and they introduced the extended form (2.4). A relation of the same form was also obtained by Collins & Chen (1970, 1971), but there appear to be some errors in the coefficients.

In the original treatment of shock dynamics for uniform media (Whitham 1957), a system of partial differential equations was derived based on the shock-ray network that related M, A and the ray inclination angle θ. The original work used the integrated form of (2.3) with $S = 0$ to give an A–M relation of the form

$$\frac{A}{A_0} = \frac{f(M)}{f(M_0)}, \tag{2.5}$$

where

$$f(M) = \exp\left(-\int\frac{M\lambda(M)}{M^2-1}\,\mathrm{d}M\right), \tag{2.6}$$

and A_0 and M_0 are some reference ray-tube area and Mach number, respectively. Catherasoo & Sturtevant follow this approach to extend the theory to non-uniform

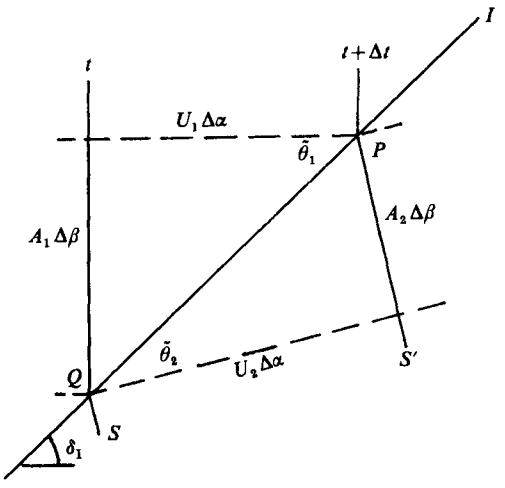

FIGURE 1. Shock wave refraction at a contact discontinuity.

media. They obtain a system of partial differential equations in characteristic form that also include the parameters of the medium. Then, they solve their partial differential equations analytically for various problems.

As noted earlier, the numerical scheme propagates the shockfront directly and bypasses the partial-differential-equation formulation. We require the A–M relation in order to determine the propagation speed for each point on the shockfront. The direction of propagation is given by the assumption in geometrical shock dynamics that points on the shockfront travel along rays normal to the shock.

2.2. *The contact discontinuity*

An important feature of these flows is the presence of jumps in the shock velocity and slope that occur at a contact discontinuity in gas properties. Accordingly, an important feature of the Catherasoo & Sturtevant theory is a new method and new expressions for these jumps. Since jumps equivalent to these will arise in the numerical solutions as well, it is useful to summarize this feature of their work.

The geometry of the situation is shown in figure 1. The gas interface I is inclined at an angle δ_1. It is assumed, for simplicity, that the ambient sound speed changes from a constant value of a_{01} to a_{02} across the interface and that all other gas properties are uniform. We see from the various ways of expressing the line segment PQ that

$$U \propto \cos\tilde{\theta}, \quad A \propto \sin\tilde{\theta}, \tag{2.7}$$

where $\tilde{\theta} = \theta - \delta_1$, and if these hold continuously across the interface, then

$$\frac{\mathrm{d}U}{U} = -\tan\tilde{\theta}\,\mathrm{d}\tilde{\theta}, \quad \frac{\mathrm{d}A}{A} = \cot\tilde{\theta}\,\mathrm{d}\tilde{\theta}. \tag{2.8}$$

By eliminating $\mathrm{d}\tilde{\theta}$, we have

$$\frac{\mathrm{d}A}{A} = -\cot^2\tilde{\theta}\frac{\mathrm{d}U}{U}. \tag{2.9}$$

The A–M relation (2.3) with (2.4) for constant p_0 and γ takes the form

$$\frac{1}{\nu^2}\frac{\mathrm{d}M}{M} + \frac{\mathrm{d}A}{A} + g\frac{\mathrm{d}a_0}{a_0} = 0, \tag{2.10}$$

where $$\nu = \frac{1}{M}\left(\frac{M^2-1}{\lambda}\right)^{\frac{1}{2}}.$$

Upon substitution of (2.9) into (2.10) and the observation that $\mathrm{d}U/U = \mathrm{d}M/M + \mathrm{d}a_0/a_0$, we obtain a differential relationship between M and a_0 that holds across the interface; it takes the form

$$\frac{\mathrm{d}M}{\mathrm{d}a_0} = \frac{\nu^2 M(U^2-gV^2)}{a_0(V^2-\nu^2U^2)}, \tag{2.11}$$

where $$U = a_0 M, \quad V^2 = K^2 - U^2,$$

$$K = \frac{U_i}{\cos\tilde{\theta}_i} = \text{constant}, \quad i = 1 \text{ or } 2.$$

If M_1 and θ_1 are known, then the unknown Mach number M_2 across the interface may be found by integrating (2.11) from a_{01} to a_{02}. The unknown ray angle $\tilde{\theta}_2$ is then given since K = constant.

In the derivation of (2.11) it is assumed that the A–M relation holds even for the abrupt changes in U, A and a_0 that occur across the interface. This is reasonable so long as the jump in θ and U is not too large. For large jumps, M_2 (and thus U_2) may not be given accurately by (2.11), since the A–M relation was derived assuming a gradual change in ray-tube area. An alternative would be to obtain jump conditions based on a three-shock theory. However, there is some difficulty due to the overabundance of local three-shock solutions to the full equations of gasdynamics so that the use of this theory is an added complication that does not appear to be worthwhile in view of the overall approximate theory.

Catherasoo & Sturtevant use their jump conditions at contact discontinuities and the usual jump conditions at shock–shocks in regions where the gas properties are uniform in order to construct solutions using characteristics for a class of problems involving a planar interface and a wedge wall boundary. Solutions found in this way will be compared with solutions obtained using the more general numerical scheme presented in §3, before we move on to more complicated problems where analytic solutions are not available.

3. Numerical scheme

In this section, we shall generalize the basic numerical scheme developed in Henshaw *et al.* (1986) for shock-wave motion in a uniform medium in order to account for possible non-uniformities in the gas properties ahead of the propagating shockfront. We shall stress the new aspects of the numerical scheme in the present work and treat only briefly the features discussed in detail in the previous paper.

The overall time-marching procedure is basically unaltered by the generalization to non-uniform media. We represent the shockfront by a discrete set of points. Each point is advanced along its unit normal with a velocity $U = a_0 M$, where the Mach number M is determined by numerically integrating the A–M relation (2.3) along rays. The integration of (2.3) is the only added feature to the numerical scheme. Points on the shockfront are removed or inserted depending on the local compression or expansion along the shockfront using the refinement scheme discussed in our previous paper. The same smoothing scheme is also used in order to dampen high-

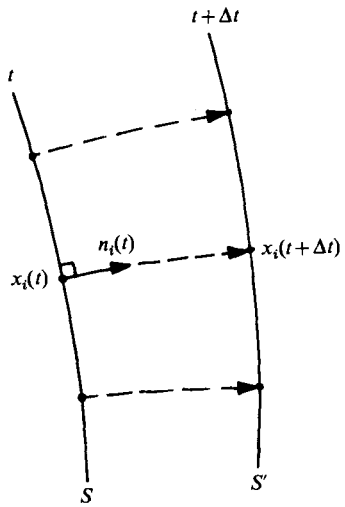

FIGURE 2. Basic time-marching scheme.

frequency numerical fluctuations in the shockfront position. A sketch of the numerical time-marching scheme is provided in figure 2.

Points $\boldsymbol{x} = (x, y)$ on the shockfront move along rays with velocity $U = a_0 M$. Therefore,

$$\frac{\partial}{\partial t}\boldsymbol{x}(\beta, t) = a_0(\beta, t) M(\beta, t)\, \boldsymbol{n}(\beta, t), \tag{3.1}$$

where $\boldsymbol{n} = (\cos\theta, \sin\theta)$ is the normal to the shockfront and β refers to the particular ray.

Discretization of (3.1) in space yields a system of N ordinary differential equations for the discrete shockfront positions $\boldsymbol{x}_j(t), j = 1, \ldots, N$. We then integrate the system of ordinary differential equations in time using the two-step leap-frog scheme

$$\boldsymbol{x}_i(t+\Delta t) = \boldsymbol{x}_i(t-\Delta t) + 2\Delta t\, a_{0i}(t) M_i(t)\, \boldsymbol{n}_i(t), \quad i = 1, \ldots, N, \tag{3.2}$$

where $t = n\Delta t$ for $n = 0, \ldots, T/\Delta t$ and $a_{0i}(t)$, $M_i(t)$ and $\boldsymbol{n}_i(t)$ are the discrete sound speed, Mach number and shockfront normal at $\boldsymbol{x}_i(t)$, respectively. The leap-frog scheme in (3.2) is neutrally stable and thus a smoothing scheme is required in order to dampen high-frequency numerical errors that accumulate over long times. We use a scheme, given in our previous paper (Henshaw *et al.* 1986), that smooths the shock position after every 25–50 time steps. We note that numerical integration schemes that smooth the shock position continuously could also have been chosen, but these schemes were not investigated, since (3.2) has proven to be a reliable choice for all our previous calculations.

The Mach number $M_i(t)$ in (3.2) is determined by numerically integrating the A–M relation (2.3) along rays. The independent variable σ in (2.3) gives the position of the shock in the channel. It is convenient to change the variable to t, the time at which a point on the shock has travelled a distance σ along its ray. We then obtain $M_i(t)$ from the integral

$$\int_0^t \left\{ \frac{M\lambda}{M^2-1}\frac{\partial M}{\partial t} + \frac{1}{A}\frac{\partial A}{\partial t} + \frac{g}{a_0}\frac{\partial a_0}{\partial t} + \frac{h}{p_0}\frac{\partial p_0}{\partial t} + k\frac{\partial \gamma}{\partial t} \right\} \mathrm{d}t = 0 \tag{3.3}$$

evaluated along the ray $\boldsymbol{x} = \boldsymbol{x}_i(t)$ for $i = 1, \ldots, N$. For simplicity, we assume that p_0 and γ are constant, then (3.3) becomes

$$-\log\frac{f(M_i(t))}{f(M_i(0))}+\log\frac{A_i(t)}{A_i(0)}+\int_0^t \frac{g(M(t))}{a_0(t)}\frac{\partial a_0}{\partial t}\,\mathrm{d}t = 0 \quad \text{for } i = 1, \ldots, N, \tag{3.4}$$

where $f(M)$ is given by (2.6), $g = g(M)$ is given in (2.4) and $A_i(t)$ is the discrete ray-tube area. The remaining integral in (3.4) is handled approximately. As a first step, we note that if $g(M) \approx g(M_0) = \text{constant}$, we can integrate to give

$$\frac{f(M_i(t))}{f(M_i(0))} = \frac{A_i(t)}{A_i(0)}\left(\frac{a_{0i}(t)}{a_{0i}(0)}\right)^{g(0)}, \tag{3.5}$$

where $g(0) \equiv g(M_i(0))$. In the numerical scheme, we can go one step better and take $g(M) \approx$ constant at each time step. This gives an A–M relation of the form

$$\frac{f(M_i(t))}{f(M_i(0))} = \frac{A_i(t)}{A_i(0)}\prod_{k=1}^{N}\left(\frac{a_{0i}(k\,\Delta t)}{a_{0i}((k-1)\,\Delta t)}\right)^{g(k-1)}, \tag{3.6}$$

where $g(k) \equiv g(M_i(k\,\Delta t))$. Inverting $f(M)$ gives $M_i(t)$, for $i = 1, \ldots, N$, and we perform this inversion numerically.

The integral in (3.4) may be approximated in a number of ways. The approximation given by (3.6) is convenient since the same numerical inversion procedure used to determine $M_i(t)$ when a_0 is constant (Henshaw *et al.* 1986) can also be used when a_0 varies. This is possible since $M_i(t)$ does not appear in the product on the right-hand side of (3.6). Other more complicated schemes may be used to approximate the integral in (3.4). However, since $g(M)$ varies slowly for $M \in [1, \infty)$, the approximate A–M relation (3.6) gives sufficient accuracy provided that the change in a_{0i} between time steps is not too large. This will be a consideration (discussed later) for problems involving a rapid change in a_0 used to approximate a contact discontinuity.

Equation (3.4) holds under the assumption that p_0 and γ are constant. If p_0 is not constant, another product term similar to the one involving a_0 would be included in (3.6). If we generalize further and let γ vary, then all but the second term in (3.3) must be treated approximately. We point out that this generalization is not particularly difficult to handle. However, we shall take the case (3.6) for simplicity in the present work.

We refer to our previous paper for the remaining details of the numerical scheme. The discrete shockfront normal $\boldsymbol{n}_i(t)$ required in (3.2) is calculated by differentiating two cubic splines fitted to the data $(s_j(t), x_j(t))$ and $(s_j(t), y_j(t))$, $j = 1, \ldots, N$, where $s_i(t)$ is the discrete arclength. Initially, the shockfront position and Mach number are given at $t = 0$. An explicit one-step scheme is used to begin the two-step leap-frog time-marching scheme. If wall boundaries are present, we require the shockfront to be normal to the walls in the numerical scheme. In expansive regions of the shockfront, points tend to spread out, and in compressive regions, points tend to cluster. We set a minimum and a maximum tolerance on the point spacing, and we insert or delete points in order to maintain this restriction.

4. Shock-wave refraction

We consider two fundamental shock-wave refraction problems. In §4.1, we discuss our calculations for shock-wave refraction at a planar interface separating two gases with constant unequal sound speeds, and in §4.2, we examine the interaction of plane

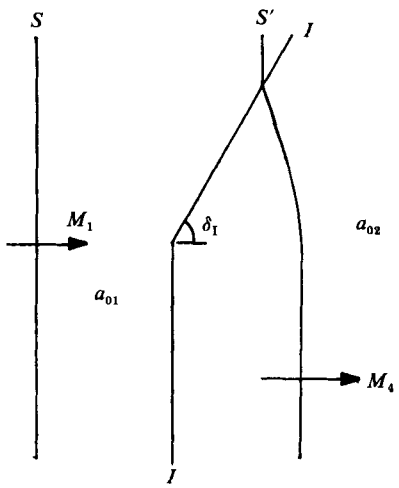

FIGURE 3. Interface geometry.

shock waves at curved gas inhomogeneities. For the planar-interface problem, theoretical and experimental studies exist and these are compared with our numerical results. For the curved-interface problem, we compare our calculations with experimental observations only; we know of no other theoretical results for this problem. For both problems, we find that the leading shockfronts determined using the approximate theory predict the actual shocks with good accuracy.

4.1. *Shock wave refraction at a planar gas interface*

We calculate the successive shock positions for the problem shown in figure 3. The interface I is composed of two planar parts. The lower part is vertical, and the upper part is inclined at an angle δ_I with the horizontal. The incident shockfront S travels towards the interface with constant Mach number M_1. The sound speed in this region is a_{01}. After contact with the interface, the shockfront S' bends to adjust to the different sound speed a_{02} on the opposite side of the interface. The curved central portion of S' originates from the refraction at the interface corner. At a sufficient distance away from the central portion, S' remains planar, travelling with constant Mach number M_1 in the upper part and M_4 in the lower part. (The subscript '4' is used for later convenience.) The case shown in figure 3 is for $a_{02} > a_{01}$.

It is possible to construct analytic solutions to the equations of geometrical shock dynamics for the problem illustrated in figure 3. These analytic solutions assume a discontinuous change in sound speed across the interface. The Catherasoo & Sturtevant jump conditions (2.11) are used to relate M and θ on either side in terms of δ_I, a_{01} and a_{02}. In our numerical description, we model the contact discontinuity by a continuous distribution of sound speed with a rapid change from a_{01} to a_{02} across the interface. The width of our interface is 0.025 (using the same scale as in the figures). Thus, if $M_1 = 5$ and $\Delta t = 0.001$, as is the case in a typical calculation, then a minimum of approximately 5 time steps are required for a point on the shockfront to traverse the interface. This minimum is needed for an accurate integration of the A–M relation and it occurs for a head-on interaction. In this case, we obtain a value of $M_4 = 3.551$ for $a_{02}/a_{01} = 2$. This compares with the exact value of $M_4 = 3.557$ which is found by numerically integrating the jump condition (2.11).

In figure 4, we display the successive shockfronts calculated using the present

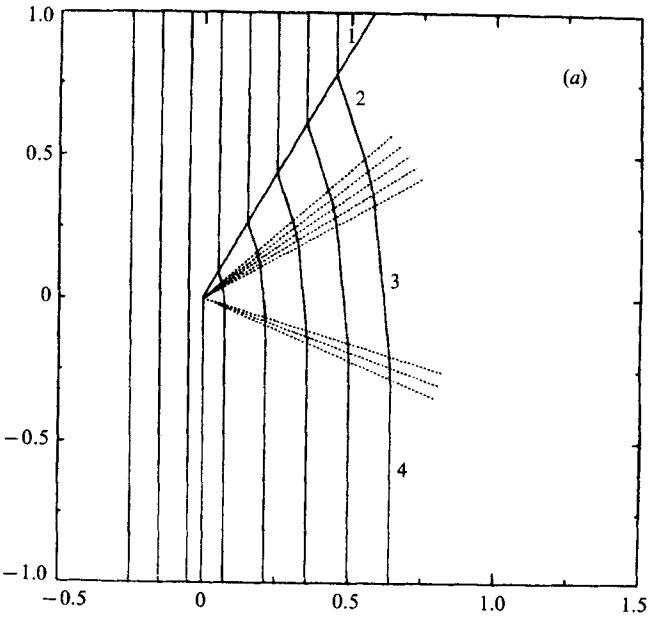

$M_1 = 5$ $M_2 = 3.73$ $M_3 = 3.40$ $M_4 = 3.56$

$\theta_1 = 0°$ $\theta_2 = 18.3°$ $\theta_3 = 6.0°$ $\theta_4 = 0°$

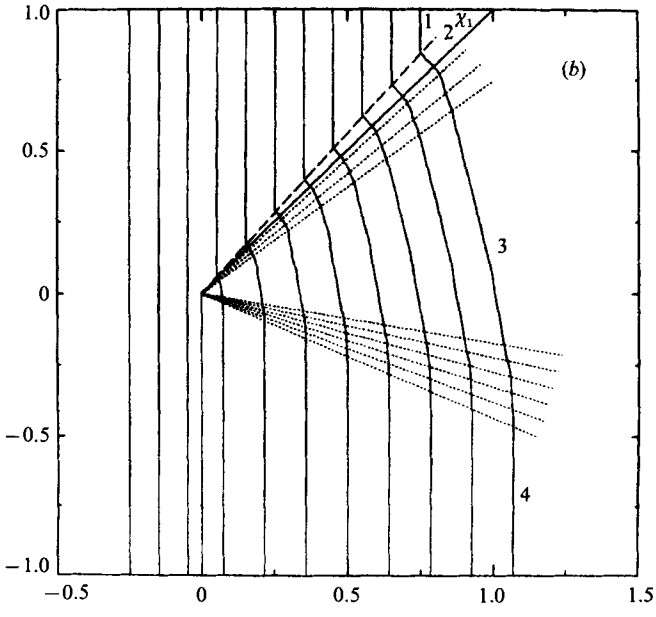

$M_1 = 5$ $M_2 = 7.44$ $M_3 = 3.21$ $M_4 = 3.56$ $\chi_1 = 48.0°$

$\theta_1 = 0°$ $\theta_2 = 42.5°$ $\theta_3 = 13.6°$ $\theta_4 = 0°$

FIGURE 4(*a*, *b*). For caption see page 394.

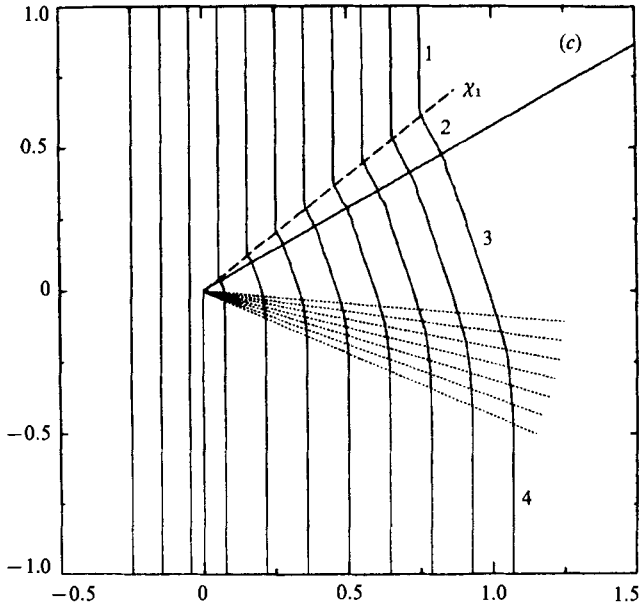

$M_1 = 5$ $M_2 = 6.33$ $M_3 = 3.10$ $M_4 = 3.56$ $\chi_1 = 39.1°$

$\theta_1 = 0°$ $\theta_2 = 28.3°$ $\theta_3 = 18.3°$ $\theta_4 = 0°$

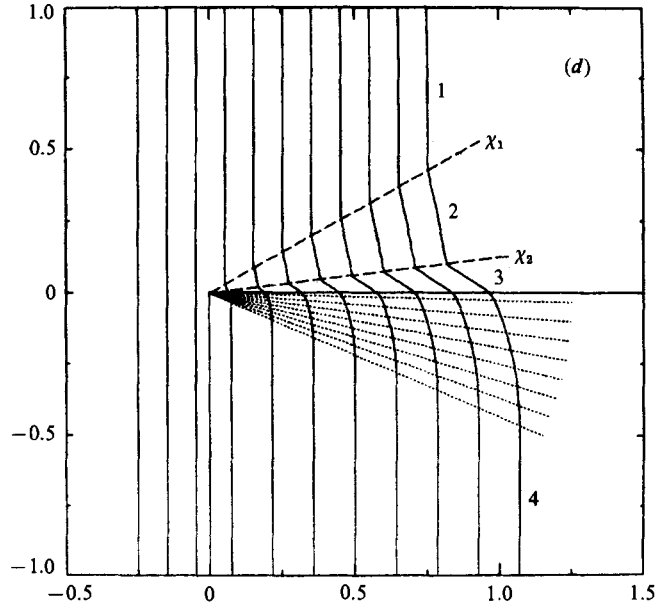

$M_1 = 5$ $M_2 = 5.47$ $M_3 = 3.53$ $M_4 = 3.56$ $\chi_1 = 29.7°$

$\theta_1 = 0°$ $\theta_2 = 11.6°$ $\theta_3 = 57.1°$ $\theta_4 = 0°$ $\chi_2 = 7.2°$

FIGURE 4(*c*,*d*). For caption see page 394.

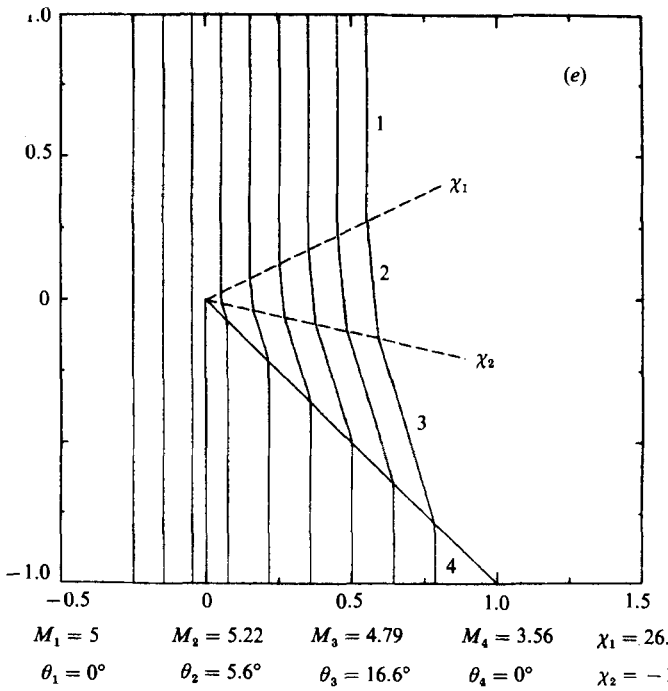

FIGURE 4. Shock-wave refraction for $M_1 = 5$ and $a_{02}/a_{01} = 2$: (*a*) $\delta_I = 60°$; (*b*) 45°; (*c*) 30°; (*d*) 0°; (*e*) −45°.

numerical scheme. The five different values of the interface inclination angle shown, $\delta_I = 60°$, 45°, 30°, 0° and −45°, are chosen to correspond to five of the many cases considered by Catherasoo & Sturtevant in their paper. For all five plots, $M_1 = 5.0$ and $a_{02}/a_{01} = 2.0$. For $\delta_1 = 60°$ (figure 4*a*), the incident planar shock wave meets the inclined interface and bends sharply forward to adjust to the larger sound speed on the other side. The refracted shockfront across the interface is composed of three regions of constant M and θ separated by two curved portions between regions 2 and 3, and between 3 and 4. These curved portions correspond to the centred expansion fans in the analytic solutions. To make this comparison, the dotted lines have been drawn in the numerical plots as an estimate of where the fans would fit. The two expansion fans are of different type, one belonging to the C_+ and the other to the C_- characteristics of the equations of geometrical shock dynamics. Two expansion fans are required in this case as waves travel in both directions along the shockfront away from the interface corner. The sharp bend in the shockfront seen at the inclined interface corresponds to the case of *regular refraction* for the shock. As δ_I decreases, the C_+ expansion fan meets the interface and a further decrease in δ_I results in the presence of a shock–shock in front of the inclined interface (as shown in figures 4*b* and 4*c*), where the locus of shock–shock positions is denoted by the dashed lines in each figure. These shockfront patterns correspond to *irregular refraction* systems for the shock. Finally, figures 4(*d*) and 4(*e*) show a second shock–shock above the interface for $\delta_1 = 0°$ and −45°. The second shock–shock belongs to the opposite family relative to the first, and it forms after the C_- expansion fan meets the interface.

In figure 4 (and also in figures 6, 7 and 10), we give the exact values of the Mach number, ray angle and shock–shock angle computed using characteristics and the

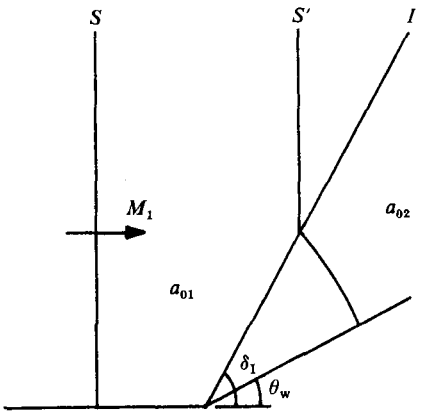

FIGURE 5. Interface–wall geometry.

appropriate jump conditions. These values are in good agreement with the ones found in our numerical calculations. For example, the exact values of M_2 and M_3 for the case shown in figure 4(*a*) are 3.73 and 3.40, respectively. The values found from our numerical results are $M_2 = 3.73 \pm 0.005$ and $M_3 = 3.40 \pm 0.01$. Catherasoo & Sturtevant also give M, θ and χ for the cases shown in figure 4; however, they incorporate the true value of $M_4 = 3.43$ as given by one-dimensional gasdynamics into their geometrical-shock-dynamics calculations in order to improve their overall results. Consequently, their value of M_3 changes to 3.34 for the case shown in figure 4(*a*); the value of M_2 is unaffected. These values compare with $M_3 = 3.40$ and $M_4 = 3.56$ as given entirely by geometrical shock dynamics. Our numerical results give these values as well, since our numerical scheme is based entirely on geometrical shock dynamics. For cases shown in figures 6, 7 and 10, where a wall boundary is added to the problem, Catherasoo & Sturtevant's results employ geometrical shock dynamics only (no added information from one-dimensional gasdynamics is available in this case) and our results are in complete agreement with theirs.

The transition from regular to irregular refraction arises naturally in the theory of geometrical shock dynamics for non-uniform media. This transition is seen in figures 4(*a*) and 4(*b*) as δ_I is decreased from 60° to 45°. As indicated earlier, the criterion for transition for this problem involves the confluence of the leading edge of the C_+ expansion fan and the interface. Let the angle between the C_+ characteristic in the region just behind the inclined interface and the horizontal be given by δ_+. This angle defines the leading edge of the C_+ expansion fan. Regular refraction occurs for $\delta_+ < \delta_I$. In this case, disturbances along the shockfront originating from the interface corner cannot propagate ahead of the C_+ expansion fan to the inclined interface. Thus, we have regions of constant M and θ on each side of the inclined interface separated by a sharp bend in the shockfront at the interface. This pattern is characteristic of regular refraction. For $\delta_+ = \delta_I = 55.7°$, the edge of the C_+ expansion fan meets the inclined interface and the constant region behind the interface vanishes. A further decrease in δ_I results in the formation of a shock–shock on the inclined interface for the small range $55.7° > \delta_I > 55.0°$. Then, for $\delta_I < 55.0°$, the shock–shock moves away from the interface, which indicates an irregular refraction system for the shock.

For the small range of δ_I between 55.0° and 55.7°, Catherasoo & Sturtevant had a gap in their set of analytic solutions. The numerical calculations, on the other hand,

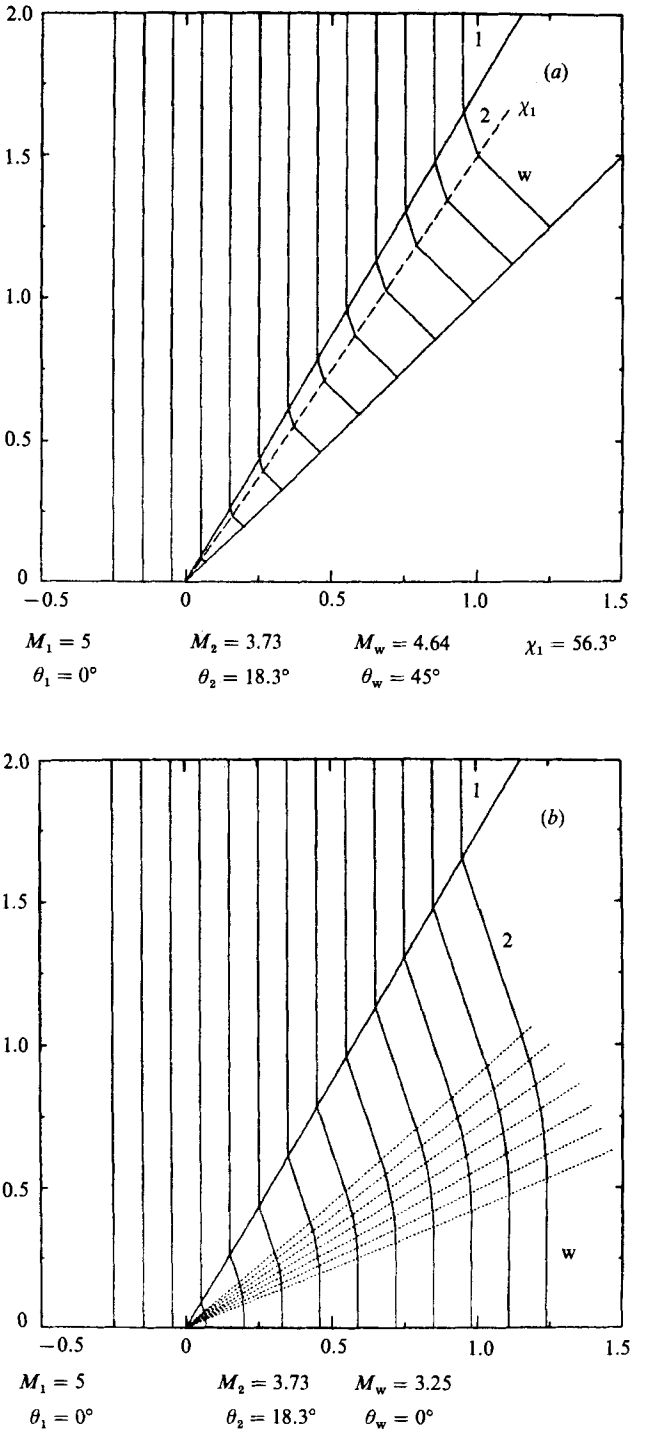

FIGURE 6(*a*,*b*). For caption see facing page.

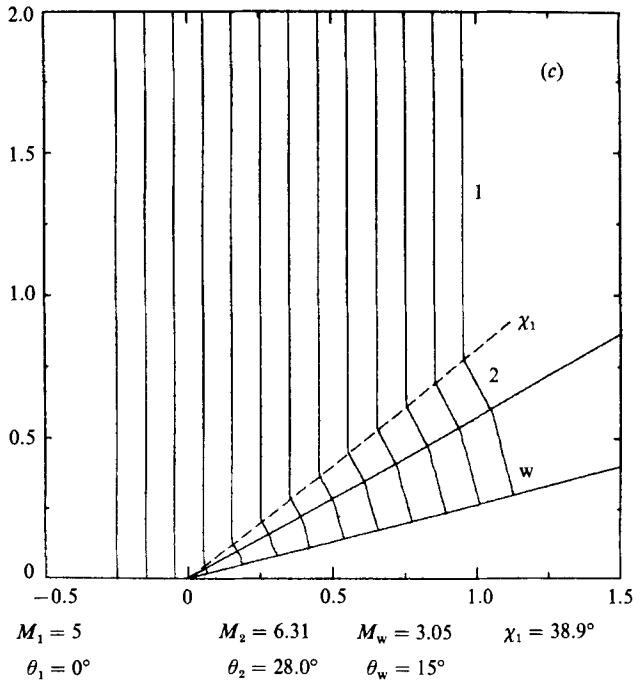

FIGURE 6. Shock-wave refraction for $M_1 = 5$ and $a_{02}/a_{01} = 2$: (*a*) $\delta_I = 60°$, $\theta_w = 45°$; (*b*) $\delta_I = 60°$, $\theta_w = 0°$; (*c*) $\delta_I = 30°$, $\theta_w = 15°$.

give solutions for all values of δ_I with no apparent difficulties. On closer examination, there appears to be a sandwich consisting of a contact discontinuity, a shock–shock, and then another contact discontinuity, with overshoots in M and θ, across the interface. This possibility was not considered by Catherasoo & Sturtevant and could now be added to complete the set of analytic solutions for this problem. This structure seems peculiar, however, and we suspect that the approximate theory with the differential A–M relation (2.10) is stretched too far in this very special case for the small range of δ_I. In reality, the layer is probably replaced by some simpler structure.

It is interesting to note that if $g(M)$ in (2.10) is taken to be constant (either $g(M_1)$, $g(M_2)$, or $g(\bar{M})$, where $\bar{M}$ is some mean value of M_1 and M_2), then the complicated structure at the interface disappears and there is a simple transition from the regular to irregular refraction patterns at a single value of δ_I. For example, if we take $g = g(M_1) = \text{constant}$, where $M_1 = 5.0$, then the transition occurs at $\delta_I = 55.4°$. Mathematically, this difference between the choice of the original function $g(M)$ and $g = \text{constant}$ concerns the integrability of the Pfaffian form (2.10). If g is a function of M, then (2.10) is not integrable and any transition from (M_1, A_1, a_{01}) to (M_2, A_2, a_{02}) depends on the integration path, i.e. the assumed relation between A and a_0 during transition. If $g = \text{constant}$, however, (2.10) integrates to give

$$\frac{f(M_2)}{f(M_1)} = \frac{A_2}{A_1}\left(\frac{a_{02}}{a_{01}}\right)^g, \tag{4.1}$$

where $f(M)$ is given in (2.6). In this case, the relation between end points is independent of path and it is presumably not subject to the extreme sensitivity that

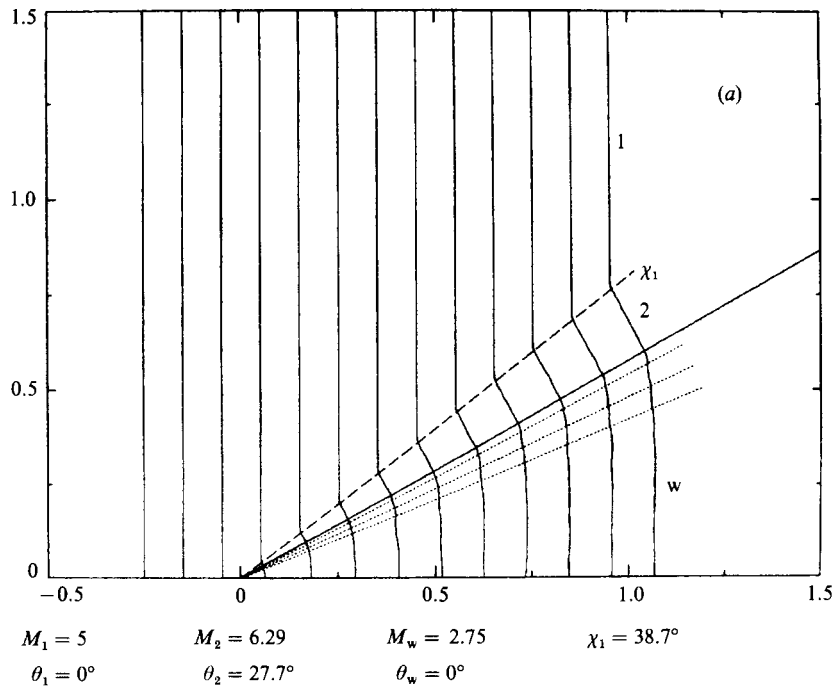

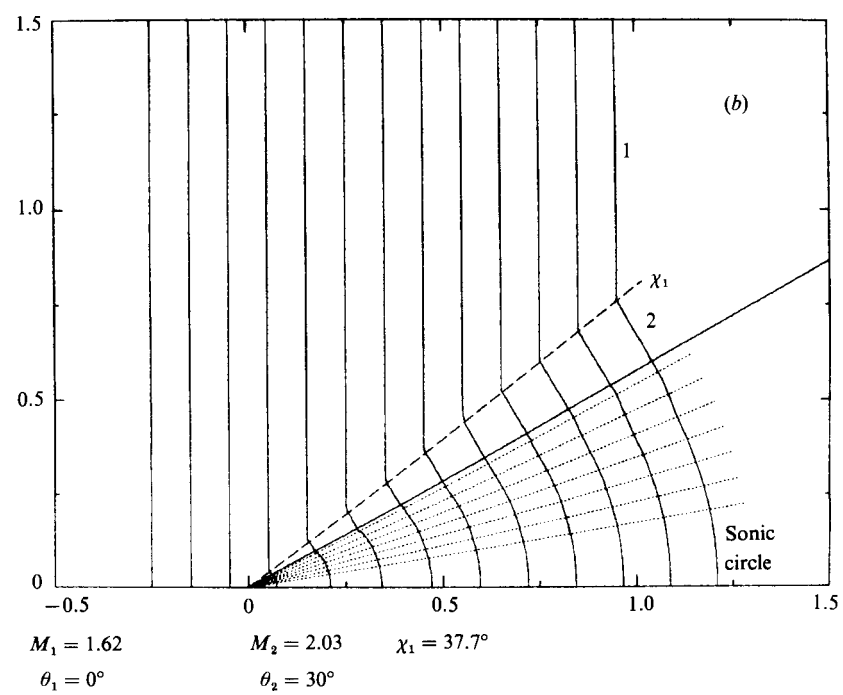

FIGURE 7 (a, b). For caption see facing page.

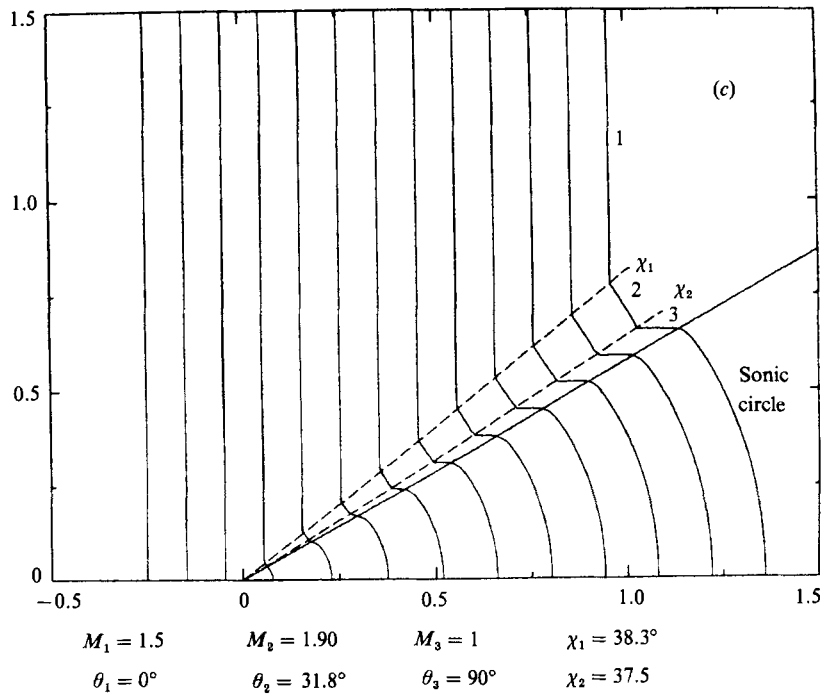

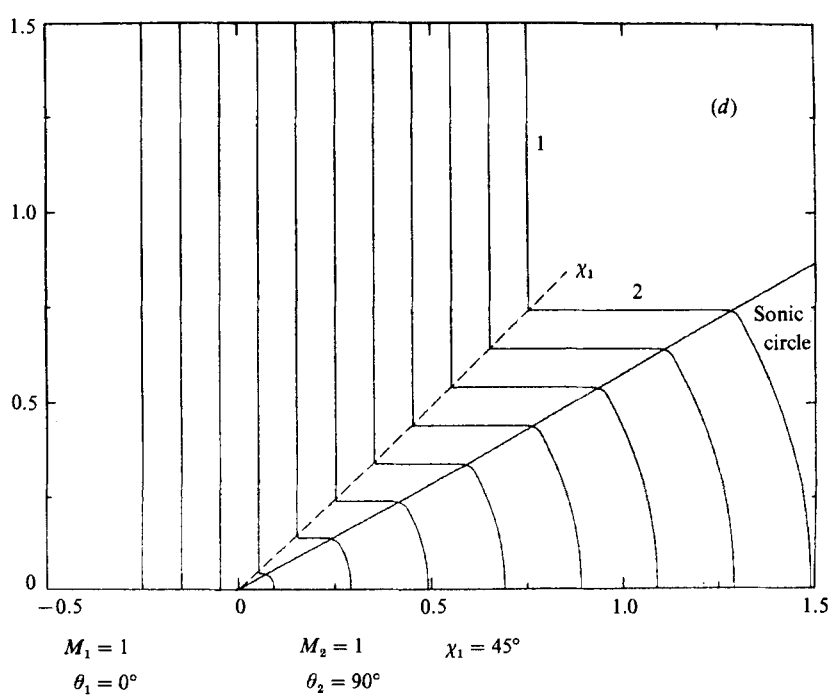

FIGURE 7. Shock-wave refraction for $\delta_1 = 30°$, $\theta_w = 0°$ and $a_{02}/a_{01} = 2$: (*a*) $M_1 = 5.0$; (*b*) 1.62; (*c*) 1.50; (*d*) 1.

occurs otherwise for the special case, and the small range of δ_I, when a shock–shock forms on the interface.

The refracted shockfronts for $a_{02} > a_{01}$, the so-called 'slow–fast' interface, are displayed in figure 4. We do not discuss the 'fast–slow' interface for this simple problem, since the shockfront patterns for the two cases are similar and no new information is gained.

The geometry of the second planar-interface problem that we study is shown in figure 5. This problem is similar to the previous one except for the addition of a wedge. Exact similarity solutions to the equations of geometrical shock dynamics using the Catherasoo & Sturtevant jump conditions across the interface are available for this problem also, and these solutions can be constructed exactly as before where we now include the boundary condition at the wall. The incident shock wave S travels along the wall with constant Mach number M_1. The planar interface I is inclined with an angle δ_I. The wedge angle is given by θ_w, and the Mach number along the inclined wall is denoted by M_w. The sound speed on either side of the interface is constant and given by a_{01} and a_{02} as before.

Three typical examples of the shockfronts calculated for the second problem are given in figure 6(*a–c*). In all three cases, $a_{02} > a_{01}$. For $\delta_I = 60°$ (figure 6*a*, *b*), we see a sharp bend in the shockfront at the interface, characteristic of regular refraction. The refracted shockfront just behind the interface is planar with $M = 3.73$ and $\theta = 18.3°$. For $\theta_w = 45° > 18.3°$ (figure 6*a*), the wedge creates a compressive turning of the shock, and thus a shock–shock forms in the region behind the interface. The opposition situation is shown in figure 6(*b*) where $\theta_w = 0° < 18.3°$. In this case, the refracted front adjusts to the wall through a centred expansion in M and θ along the shockfront. Depending on δ_I and θ_w, it is also possible to obtain irregular refraction patterns as shown, for example, in figure 6(*c*). We note that the values given in figure 6 all agree with the ones reported by Catherasoo & Sturtevant.

In all cases considered so far, we have examined the behaviour of the shockfronts for fixed initial shock strength and varying interface–wall geometry. It is also interesting to study the effect of decreasing the initial shock strength while holding the interface–wall geometry fixed. We display the effect of decreasing M_1 in figure 7. The particular interface–wall geometry chosen is $\delta_I = 30°$ and $\theta_w = 0°$. For $M_1 = 5.0$ (figure 7*a*), a single shock–shock is seen ahead of the interface. The shockfront behind the interface is composed of a centred expansion just behind the interface and a planar portion near the wall. As M_1 is decreased, the expansion fan grows until it meets the wall for $M_1 = 1.64$. The wall Mach number also decreases from $M_w = 2.8$ for $M_1 = 5.0$ to $M_w = 1$ for $M_1 = 1.64$. A further decrease in M_1 results in the formation of a sonic circle attached to the wall as shown in figure 7(*b*). (We determine the presence and extent of the sonic circle using our numerical calculations by checking the variation of M and θ along the shockfront.) In this case, the expansion along the shockfront is completed prior to the wall (i.e. M decreases to 1 before the wall), and the remaining portion of the front is sonic. This is exactly the same situation that occurs in the approximate theory for very weak shock diffraction by an expansive corner. For $M_1 = 1.60$, the sonic circle fills the region behind the interface, and for $M_1 < 1.60$ (figure 7*c*), we observe a second shock–shock and a *precursor wave* with $M_p = 1$, in region 3, just in front of the interface. The precursor wave connects the sonic circle behind the interface with the incident shock through a series of two shock–shocks of opposite type. We will show that the sonic circle and the precursor wave are the same ones as those given in geometrical acoustics. The Mach stem between the two shock–shocks is the characteristic opening of a corner in

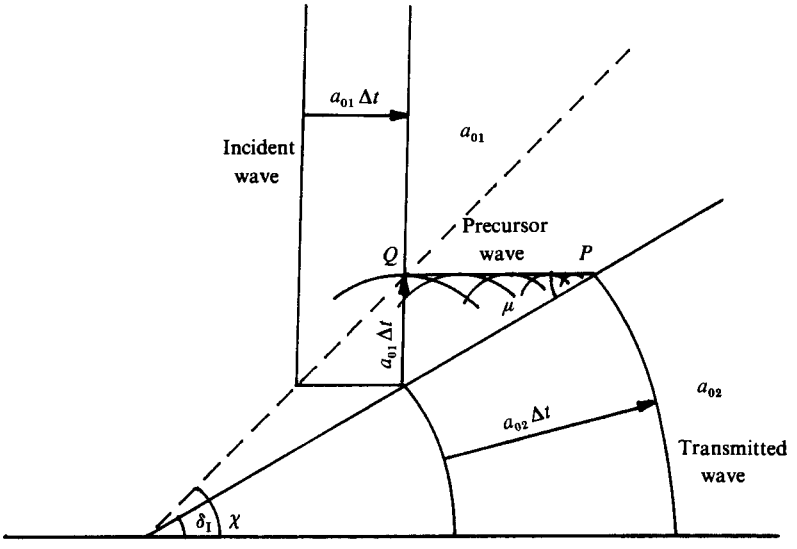

FIGURE 8. Shock-wave refraction for $\delta_I = 30°$, $\theta_w = 0°$ and $a_{02}/a_{01} = 2$: geometrical acoustics.

geometrical shock dynamics. We show the limiting acoustic case calculated using our numerical scheme with $M_1 = 1$ in figure 7(*d*).

An independent check of our numerical calculations is made by comparing them with the established results for geometrical acoustics. In figure 8, we show the leading fronts as predicted by geometrical acoustics. The transmitted wave is a sonic circle that is generated by the interface–wall corner. It moves with speed a_{02} in medium 2. The transmitted wave, in turn, radiates circular disturbances, centred at the moving point P, that propagate back into medium 1 with speed a_{01}. The envelope of these circular disturbances forms the planar precursor wave, inclined at the Mach angle

$$\mu = \arcsin\left(\frac{a_{01}}{a_{02}}\right) \tag{4.2}$$

with respect to the interface, as shown in figure 8. For $a_{01}/a_{02} = \frac{1}{2}$, $\mu = 30°$, and this agrees with the value shown in figure 7(*c*) and (*d*). A corner (shock–shock) is present at the point Q where the precursor wave meets the incident front. The locus of these corner positions forms a line inclined at an angle χ given by

$$\chi = \tfrac{1}{4}\pi + \tfrac{1}{2}(\delta_I - \mu). \tag{4.3}$$

As noted earlier, the sonic circle and precursor wave in figure 7(*c*) and (*d*) have $M = 1$ and these agree with the corresponding fronts given by geometrical acoustics. The corner opens up into a Mach stem in the geometrical-shock-dynamics plot since $M_1 = 1.5 > 1$. For $M_1 = 1$ (figure 7*d*), the Mach stem vanishes and our numerical results are in complete agreement with geometrical acoustics.

The precursor shockfront pattern shown in figure 7(*c*) has not been obtained from the approximate theory previously. Catherasoo & Sturtevant give analytic solutions using the same interface–wall geometry for M_1 between 5.0 and 1.77 in agreement with our results. For $M_1 < 1.77$, they were unable to construct solutions to the equations of geometrical shock dynamics. They hypothesized correctly that the limit corresponded to the formation of a precursor-irregular refraction pattern. However, their method of constructing solutions required some initial choice of the form of the

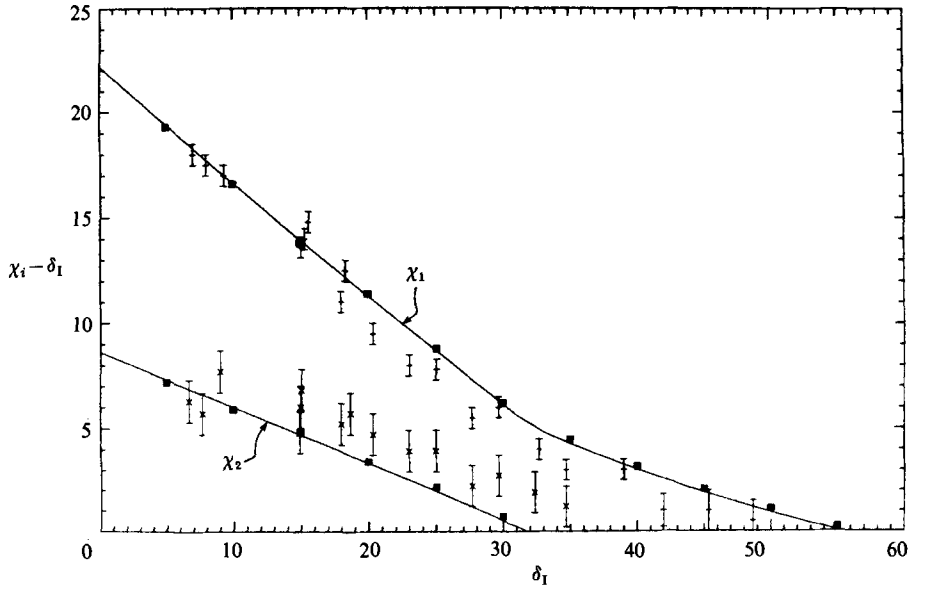

FIGURE 9. Comparison of shock–shock positions for $M_1 = 1.34$ and $a_{02}/a_{01} = \frac{5}{3}$: ——, exact shock–shock positions; ■, numerical shock–shock positions; ⊤ and ⊥, experimental triple-point positions for χ_1 and χ_2, respectively.

solution, before an iteration procedure could be applied until all of the equations (jump conditions and characteristic equations) were satisfied simultaneously. The present numerical scheme requires no prior knowledge of the solution. This exemplifies one advantage of using the general numerical scheme presented in §3. Furthermore, for these relatively simple geometries, we are lead to the correct form of the analytic solutions from our numerical calculations.

Overall, the refracted shockfronts found using geometrical shock dynamics are in good agreement with experimental results. A detailed comparison with the experimental data of Jahn (1956), Abd-el-Fattah *et al.* (1976) and Abd-el-Fattah & Henderson (1978) may be found in Catherasoo & Sturtevant's paper. Generally Catherasoo & Sturtevant showed that geometrical shock dynamics is able to predict the transition from regular to irregular refraction accurately, as well as giving accurate triple-point (shock–shock) positions. We add a further comparison between our new precursor-irregular refraction patterns and the corresponding ones observed experimentally by Abd-el-Fattah & Henderson.

Abd-el-Fattah & Henderson (1978) experimentally examined the interaction of plane shocks at an inclined gas interface. They studied a slow–fast interface using methane and carbon dioxide, so that $a_{02}/a_{01} = 5/3$ ideally, but there is always some leakage across the interface. They present results obtained for three different initial shock strengths, $M_1 = 1.12$, 1.34 and 2.24, which were representative of their very weak group, weak group and strong group, respectively. In agreement with our results, they observe regular refraction for large δ_I, with transition to various irregular refraction systems occurring for smaller δ_I. Their study emphasized the many irregular refraction systems possible for this problem, and in particular, they observe the same precursor-irregular refraction patterns as the one shown in figure 7(*c*).

We compare the shock–shock angles found using the approximate theory with the

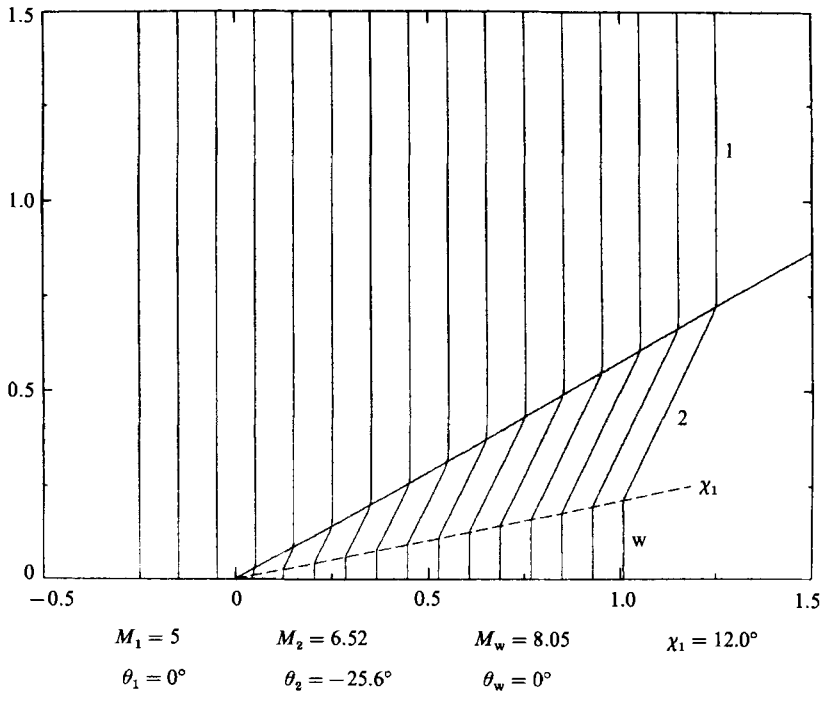

FIGURE 10. Shock-wave refraction for $M_1 = 5$, $\delta_I = 30°$, $\theta_w = 0°$ and $a_{02}/a_{01} = 0.5$.

experimental triple-point positions in figure 9. We use $M_1 = 1.34$ and we assume that $a_{02}/a_{01} = 5/3$. The two curves in figure 9 give the variation of the two shock–shock angles, χ_1 and χ_2, with δ_I. (The corresponding shockfront pictures are similar to the ones shown in figure 7*a–d*.) These curves are found from the analytic solutions constructed using characteristics and the appropriate jump conditions. We also find χ_1 and χ_2 using our numerical scheme and these are plotted in figure 9 as well. The experimental points were extracted from Abd-el-Fattah & Henderson's paper and the error bars give an indication of the reported experimental error. We note the good agreement for χ_1. The agreement for χ_2 appears to be best for smaller δ_1, where the difference $\chi_2 - \delta_I$ is largest. For smaller values of $\chi_2 - \delta_1$, there is some small discrepancy between the theoretical and experimental points. It is possible that this difference is due to the difficulty in distinguishing the triple-point position in photographs when the triple-point is near the interface. This difficulty was suggested by Abd-el-Fattah & Henderson in their paper. Overall, the agreement is remarkable considering the relatively simple approximate theory involved.

Before moving on to the next problem, we display a representative picture of the refracted shockfronts for $a_{02} < a_{01}$, the 'fast–slow' interface (figure 10). For the example shown, $\delta_1 = 30°$, $\theta_w = 0°$ and $a_{02}/a_{01} = 0.5$. The shockfront bends sharply backwards at the interface as the shockfront enters the region of 'slower' gas. The adjustment to the boundary condition at the wall is made through a shock–shock. This pattern is characteristic of all the cases considered for a_{02}/a_{01}.

4.2. *Shock-wave refraction at curved gas interfaces*

In this subsection, we study the case of shock-wave refraction at a gaseous interface of cylindrical or spherical geometry. These problems contain at least one lengthscale,

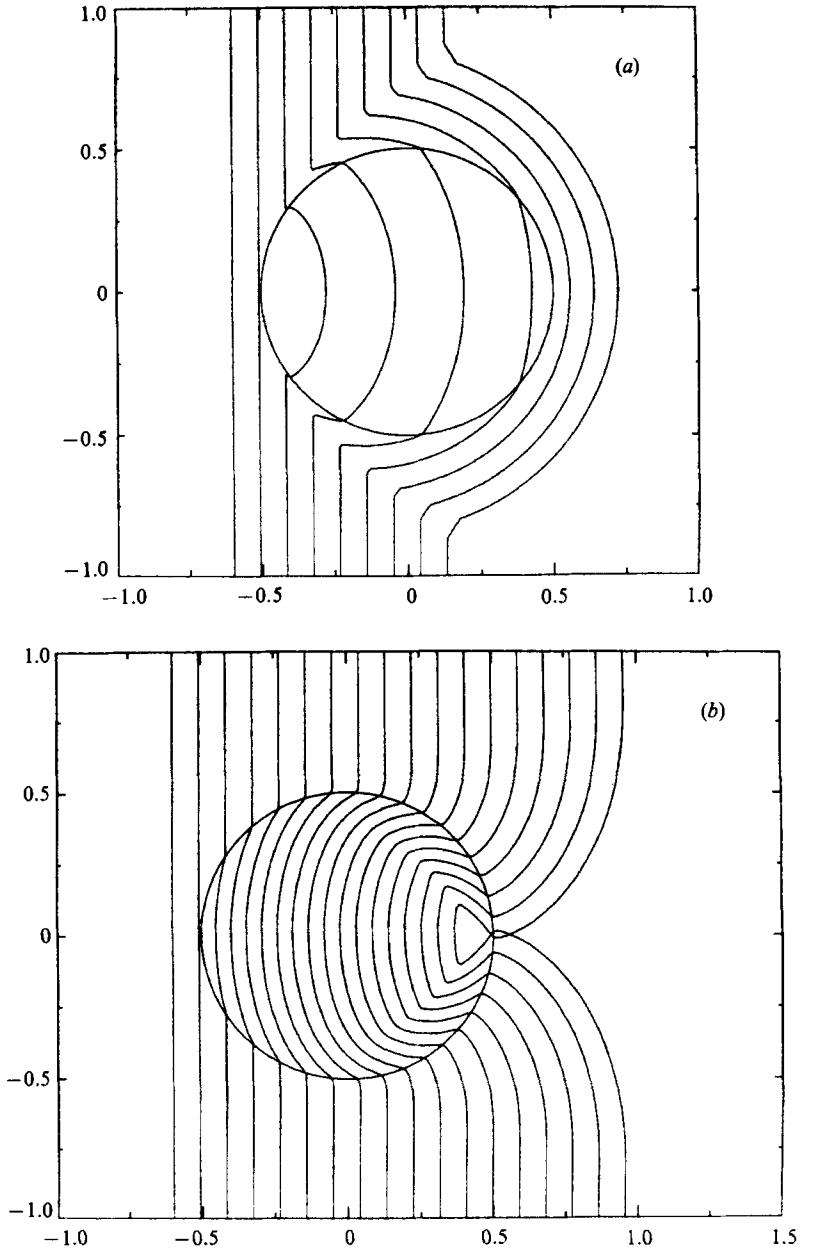

FIGURE 11. Shock-wave refraction at a cylindrical interface for $M_1 = 1.22$ and $R_1 = 0.01$; (a) $a_{02} = 2.9$ (helium-filled cylinder); (b) $a_{02} = 0.53$ (freon-filled cylinder).

namely, the radius of the cylinder or sphere, as opposed to the two self-similar problems previously considered. This fact presents no added difficulty for our numerical scheme. The method of constructing solutions using characteristics, however, is much more difficult, since there exist regions of non-trivial shock geometries and strengths. This problem is motivated by experimental results only; no theoretical results are available.

Haas & Sturtevant (1987) experimentally investigated the problem of shock-wave

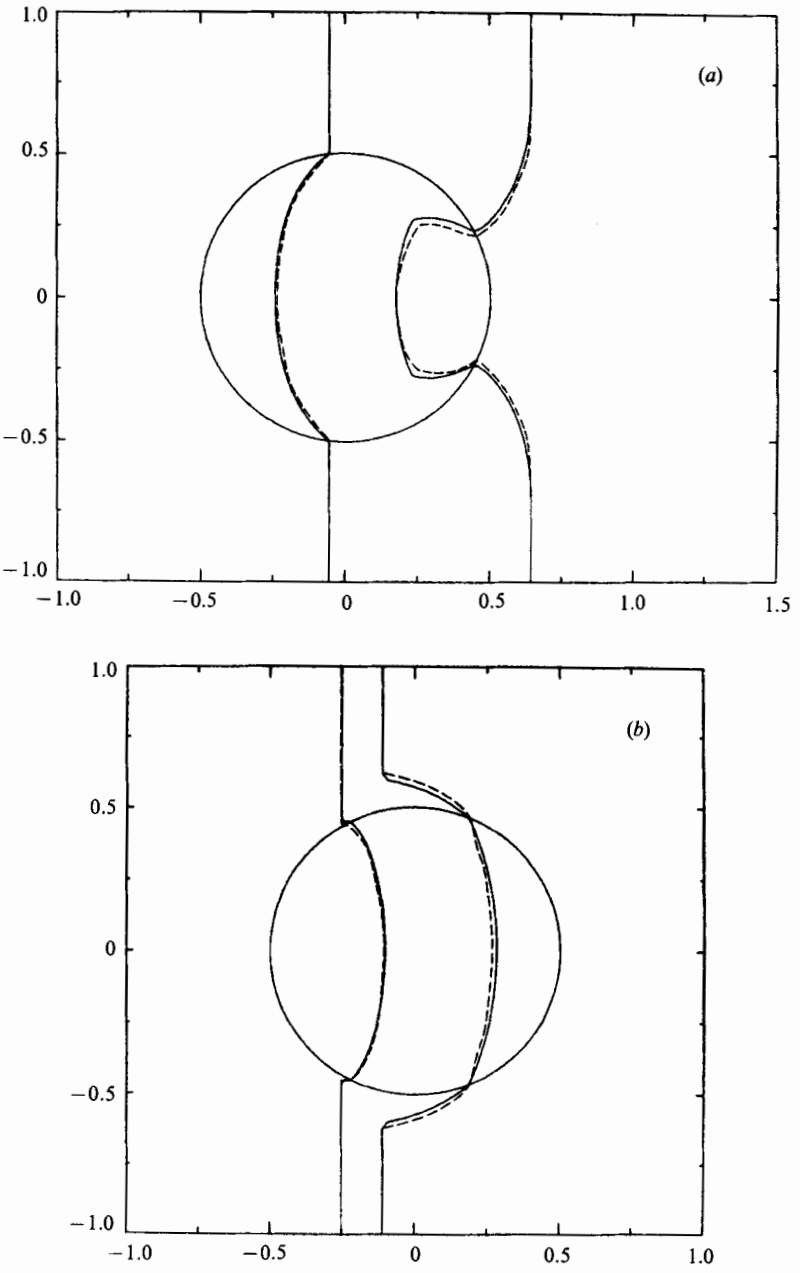

FIGURE 12. Comparison of shockfront positions for $M_1 = 1.22$ and $R_1 = 0.01$. The solid curves are the numerical results and the dashed curves are the experimental results (Haas & Sturtevant 1987). (*a*) Freon-filled cylinder; (*b*) helium-filled cylinder.

refraction by cylinders and spheres. Cylindrical membranes or spherical bubbles were filled with helium or freon-22 and suspended in a shock tube. Weak planar shock waves (incident Mach number $\leqslant 1.25$) were propagated down the shock tube. The shock-wave refraction patterns and interface deflections were observed. For the present work, we are mainly interested in the shockfront patterns observed experimentally by Haas & Sturtevant. In the case of a helium-filled cylinder or

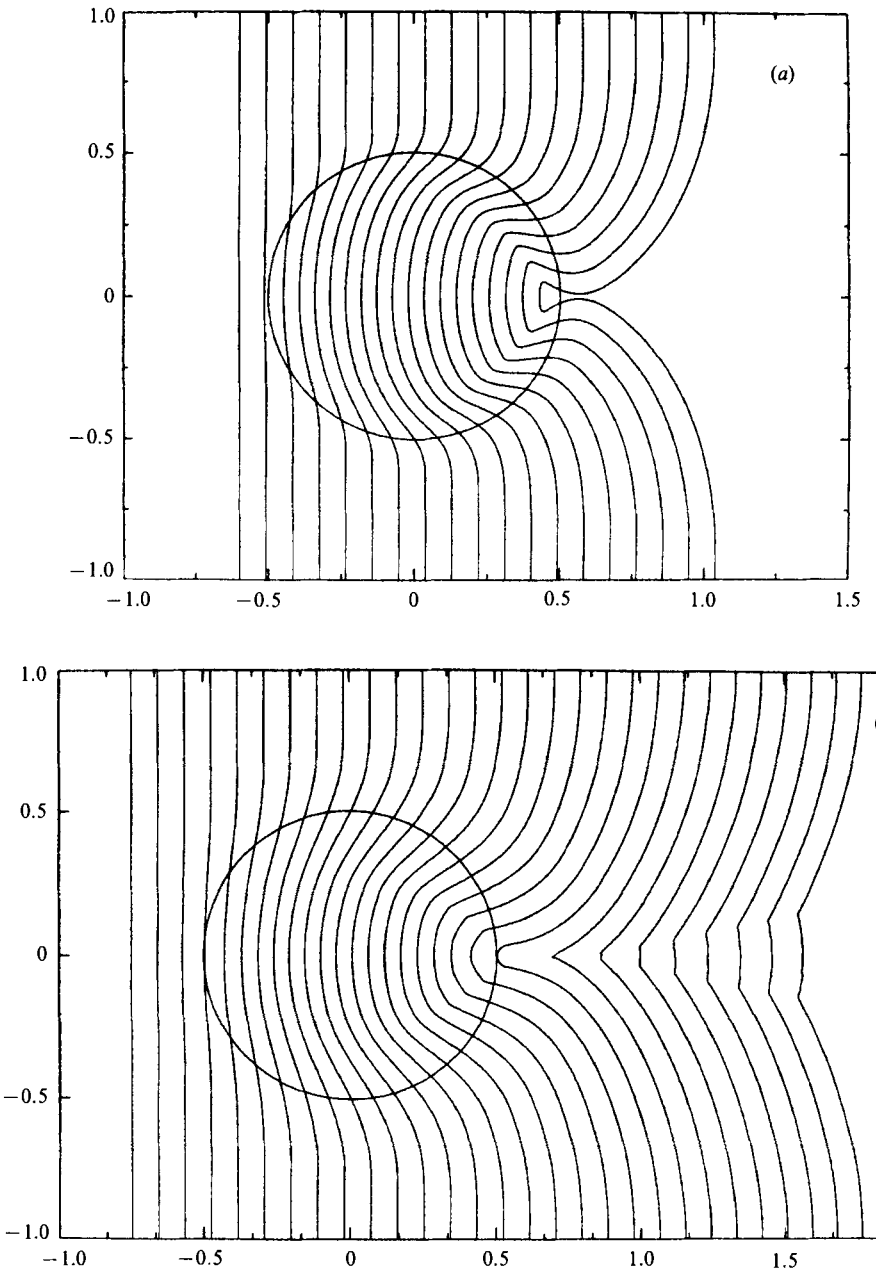

FIGURE 13(*a*,*b*). For caption see facing page.

sphere, the incident shockfront bulged forward as it crossed the interface, since the sound speed of helium (a_{He}) is greater than that of air (a_{air}). Regular refraction at the interface was observed during the initial stages of the interaction. Later, transition to irregular refraction was seen as a triple-point (shock–shock) formed near the interface in the surrounding air. For the freon-filled cylinder or sphere, the refracted shockfront lagged behind the incident front, since $a_{\mathrm{freon}} < a_{\mathrm{air}}$. Regular refraction

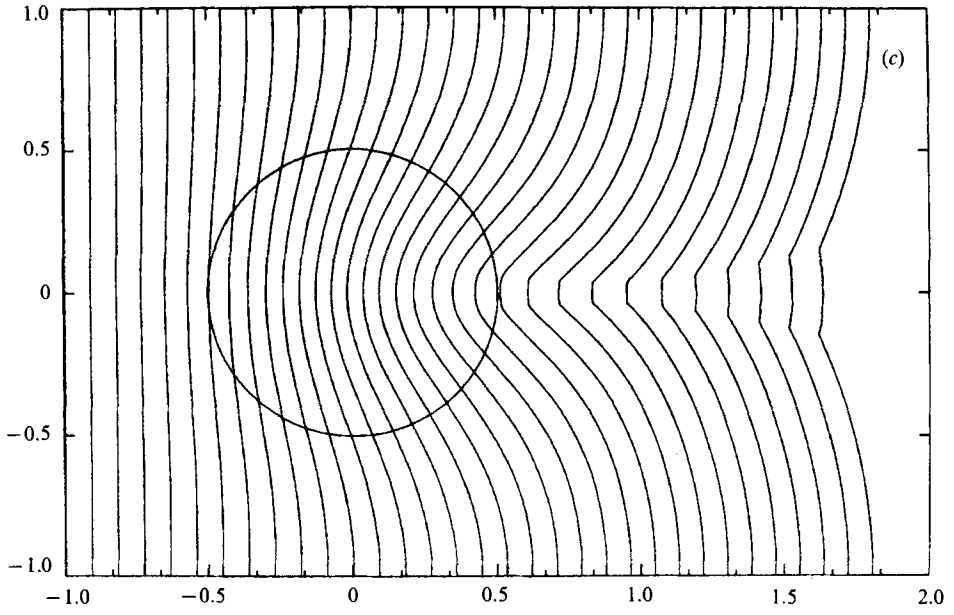

FIGURE 13. Shock-wave refraction at a cylindrical interface for $M_1 = 1.22$ and $a_{02} = 0.53$: (*a*) $R_I = 0.1$, (*b*) $R_I = 0.25$, (*c*) $R_I = R = 0.5$.

was always present at the interface. Inside the cylinder or sphere, strong internally diffracted shockfronts were observed. These waves focused and crossed as they neared the back of the cylinder or sphere.

In their paper, Haas & Sturtevant note that there was leakage across the air–freon and air–helium interfaces. For the air–freon interface, this leakage was small, resulting in an estimated 4% increase in sound speed at most inside the freon volumes. In the case of air–helium, however, they reported significant leakage so that the speed of sound inside the helium volumes was decreased by an estimated 20% (for the spherical case) depending on the particular run. These estimates were obtained by comparing the nearly planar shockfronts near the axis of symmetry with the known results for one-dimensional gasdynamics. Later in this section, we shall show that the agreement between their experimental results and our numerical results is excellent for the air–freon case, and then we shall use our numerical results to gain a better estimate of the sound speed inside the cylinders in the air–helium case.

We first treat the case of shock-wave refraction by a cylindrical interface. We use the following distribution of sound speed for the present calculations:

$$a_0(r) = \begin{cases} 1 & \text{if } r-R \geqslant R_I; \\ \frac{1}{2}\left[(1+a_{02})+(1-a_{02})\sin\left(\frac{\pi}{2}\frac{r-R}{R_I}\right)\right] & \text{if } |r-R| < R_I; \\ a_{02} & \text{if } r-R \leqslant -R_I, \end{cases} \tag{4.4}$$

where r is the radial distance from the centre of the cylinder, R is the radius of the cylinder and R_I measures the width of the cylindrical interface. The sound speed inside the cylinder is a_{02}, and the sound speed outside is normalized to 1. For the first

set of results, we take $R_I = 0.01$ to compare with experimental observations, where the cylindrical interface is thin. Later, we study shock-wave refraction for varying R_I.

In figure 11 (*a*), we show our results for the helium-filled cylinder. For helium, the normalized sound speed a_{02} in (4.4) is 2.9, ideally. This value will be reduced when comparing more closely with the experiments where a significant leakage across the interface was reported. At present, we are interested in the qualitative picture of the shockfronts. The incident Mach number is 1.22, which was also used experimentally. Near the cylindrical interface, the behaviour of the refracted shockfront is similar to those seen for the planar interface. Regular refraction is observed when the shockfront first meets the interface, since the interface inclination angle is large. As this angle decreases, transition to irregular refraction is observed. These flow features were also found experimentally by Haas & Sturtevant. The shockfront emerges from the cylinder convex forward. The helium-filled cylinder acts as a divergent lens for planar incident shock waves.

We display the calculations for the freon-filled cylinder in figure 11 (*b*). For freon-22, $a_{02} = 0.53$, and we use $M_0 = 1.22$ as before. The freon-filled cylinder acts as a convergent lens in gasdynamics. The central portion of the incident shockfront refracts at the cylindrical interface. The refracted shockfront is concave forward. The edges of the refracted front are turned more rapidly than the central portion by the faster travelling shockfront outside of the cylinder. As a result, two focusing shockfront systems (similar to the focusing shockfronts discussed in Henshaw *et al.* 1986) are seen inside the cylinder. If a_{02} is small enough, as is the case here, the shockfronts on the interface cross before the refracted shockfront reaches the back of the cylinder. All of these features are observed experimentally by Haas & Sturtevant. In particular, they note the strong internally diffracted waves predicted by geometrical acoustics. These waves are also given by geometrical shock dynamics. They are the rapidly turning edges of the refracted shockfront seen in figure 11 (*b*).

A closer comparison with the experiments of Haas & Sturtevant is shown in figure 12. In each plot, we sketch two shockfronts (dashed curves) from the photographs provided by Haas & Sturtevant for the freon-filled cylinder (figure 12*a*) and for the helium-filled cylinder (figure 12*b*). The incident Mach number in both cases is $M_1 = 1.22$, and this value is used in the numerical calculations also. The corresponding numerical shockfronts (solid curves) are plotted at the integration step when they overlap with the experimental shockfront in the undisturbed region away from the cylinder. For the freon-filled cylinder, we use the ideal value of $a_{02} = 0.53$, and we see that the agreement between the numerical and experimental shockfronts is excellent. The leakage at the freon–air interface was small in the experiments, and thus we expect this good agreement. For the helium-filled cylinder, the numerical results agree with the experimental shockfronts when a sound speed less than the ideal value for helium is used. Moreover, the two numerical shockfronts are obtained from separate calculations using two different values of a_{02}. For the shockfront on the left, $a_{02} = 1.7$, and for the one on the right, $a_{02} = 2.2$. Thus, we see that leakage at the helium–air interface for the cylinder was even greater than the 20% reported for the sphere, and since each experimental shockfront was from a different run, we find that the deviation in sound speed for each run was also large.

A further study of the refraction process is obtained by varying the interface thickness R_I in (4.4). This study has not been performed experimentally. In figure 13, we vary R_I from $R_I = 0.1$ to $R_I = R = 0.5$. The incident Mach number is $M_0 = 1.22$ and the sound speed inside the cylinder is $a_{02} = 0.53$. The case of a sharp jump in

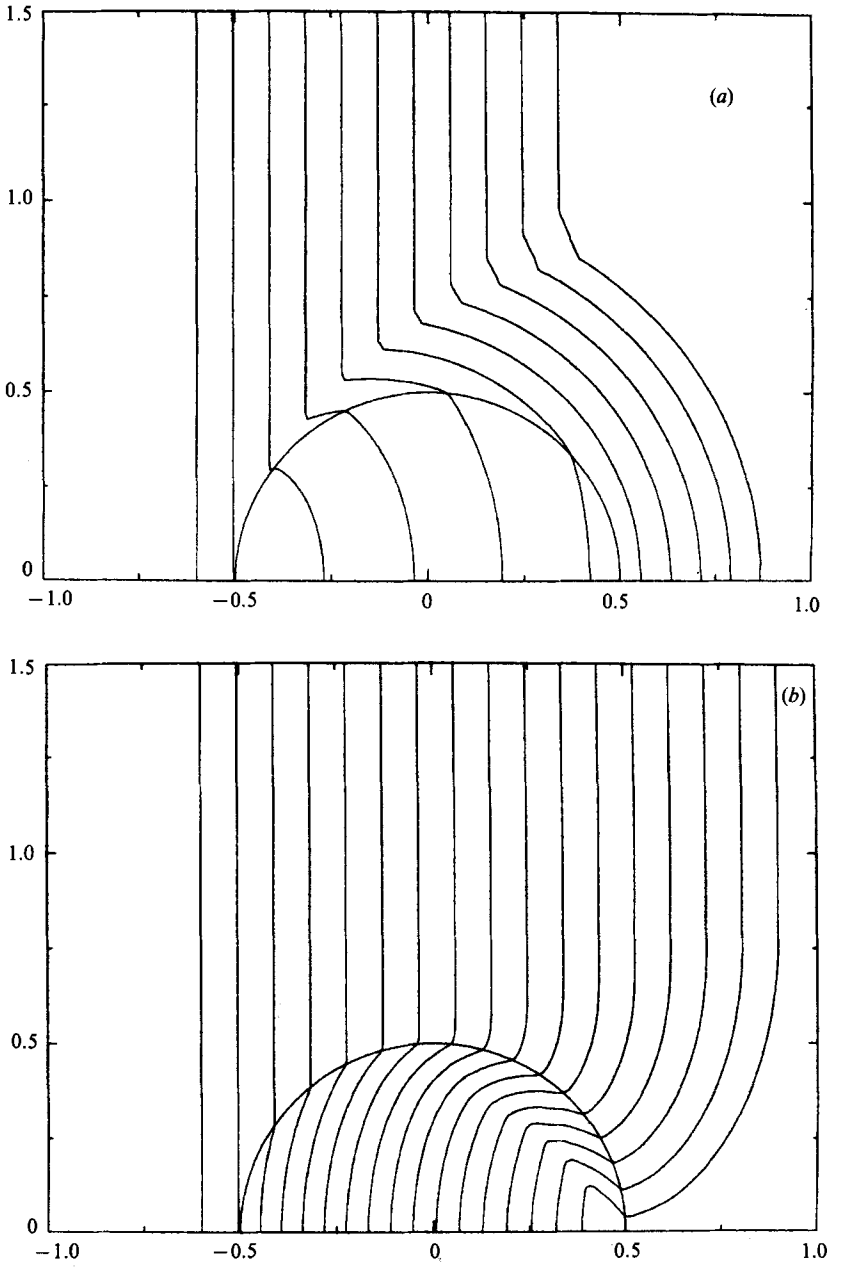

FIGURE 14. Shock-wave refraction at a spherical interface for $M_1 = 1.25$ and $R_I = 0.01$: (*a*) $a_{02} = 2.9$ (helium-filled sphere); (*b*) $a_{02} = 0.53$ (freon-filled sphere).

sound speed at the cylindrical interface ($R_I = 0.01$) is shown in figure 11(*b*). In all three pictures, we plot a circle of radius R for reference. For $R_I = 0.01$ (figure 11*b*), we noted the strong internally diffracted waves inside the cylinder. These waves crossed near the back of the cylinder. As R_I is increased, these waves are less pronounced, resulting in a weaker focus for the refracted shockfront near the back of the cylinder. The three different values of R_I shown in figure 13 (*a–c*) give the three different types of focusing. For $R_I = 0.1$, the refracted shockfronts cross near the

back of the cylinder. The refracted shockfronts for $R_I = 0.25$ emerge from the cylinder uncrossed and later focus to form a single shock–shock on the axis of symmetry. Farther downstream the single shock–shock opens up to form a pair of shock–shocks with a joining Mach stem. The weakest focusing is observed for $R_I = R = 0.5$ (figure 13*c*) as the refracted front forms a pair of shock–shocks and a Mach stem initially behind the cylinder.

For completeness, we show the shock-wave refraction patterns given at a spherical interface. The variation in sound speed given by (4.4) for the cylinder case is also used here. The diverging case ($a_{02} = 2.9$) is displayed in figure 14(*a*), and the converging case ($a_{02} = 0.53$) is given in figure 14(*b*). We take $M_0 = 1.25$ for both plots. These cases were also considered experimentally by Haas & Sturtevant. The refraction process for the sphere is found to be very similar to that of the cylinder (figure 11). Photographs of the refraction process for the actual shock waves show this similarity as well.

I would like to thank Professor G. B. Whitham for his helpful advice and for many useful discussions concerning the work presented in this paper. This research was performed at the California Institute of Technology and was supported by the Office of Naval Research, U.S. Navy. The numerical calculations were performed on the Caltech Applied Mathematics IBM 4341 computer using time donated by the IBM corporation.

REFERENCES

ABD-EL-FATTAH, A. M. & HENDERSON, L. F. 1978 Shock waves at a slow–fast gas interface. *J. Fluid Mech.* **89**, 79–95.

ABD-EL-FATTAH, A. M., HENDERSON, L. F. & LOZZI, A. 1976 Precursor shock waves at a slow–fast gas interface. *J. Fluid Mech.* **76**, 157–176.

CATHERASOO, C. J. & STURTEVANT, B. 1983 Shock dynamics in non-uniform media. *J. Fluid Mech.* **127**, 539–561.

COLLINS, R. & CHEN, H. T. 1970 Propagation of a shock wave of arbitrary strength in two half plains containing a free surface. *J. Comp. Phys.* **5**, 415–422.

COLLINS, R. & CHEN, H. T. 1971 Motion of a shock wave through a non-uniform media. In *Proc. 2nd Int. Conf. on Numerical Methods in Fluid Dynamics* (ed. M. Holt). Lecture Notes in Physics, vol. 8, pp. 264–269. Springer.

HAAS, J.-F. & STURTEVANT, B. 1987 Interaction of weak shock waves with cylindrical and spherical gas inhomogeneities. *J. Fluid Mech.* **181**, 41–76.

HENSHAW, W. D., SMYTH, N. F. & SCHWENDEMAN, D. W. 1986 Numerical shock propagation using geometrical shock dynamics. *J. Fluid Mech.* **171**, 519–545.

JAHN, R. G. 1956 The refraction of shock waves at a gaseous interface. *J. Fluid Mech.* **1**, 457–489.

WHITHAM, G. B. 1957 A new approach to problems of shock dynamics. Part 1. Two-dimensional problems. *J. Fluid Mech.* **2**, 145–171.

WHITHAM, G. B. 1959 A new approach to problems of shock dynamics. Part 2. Three-dimensional problems. *J. Fluid Mech.* **5**, 369–386.

WHITHAM, G. B. 1974 *Linear and Nonlinear Waves.* Wiley.